Solid State Science and Technology, Vol. 32, No. 2 (2024) 68-78
https://doi.org/10.66514/ssst32-2-67-78

First-Principles Study on the Structural and Electronic Properties of Pure and Cobalt-doped α-NiS

*Wan Hazeeq Azizi Wan Khairul Annuar[1], Nur Ain Nabilah Mohamad Nor[1], Muhammad Aman Haikal Razali[1], Mohd Hazrie Samat[2], Nur Hamizah Mohd Zaki[1,2] Oskar Hasdinor Hassan[2,3], Mohamad Fariz Bin Mohamad Taib[1,2,]**

[1]*Faculty of Applied Sciences, Universiti Teknologi MARA, 40450 Shah Alam Selangor, Malaysia*

[2]*Ionic Materials and Devices (iMADE), Institute of Science, Universiti Teknologi MARA, 40450 Shah Alam, Selangor, Malaysia*

[3]*Faculty of Art and Design, Universiti Teknologi MARA, 40450 Shah Alam Selangor, Malaysia*

**Corresponding author; email: mfariz@uitm.edu.my*

Received: 29 August 2024 / Accepted: 15 November 2024

ABSTRACT

The crystal structure, average bond length, electronic charge distribution, band structure, and density of states (DOS) of pure and cobalt (Co) doped α-NiS were studied using first-principles calculation based on density functional theory with the addition of Hubbard *U* (DFT+U) with Local Density Approximation with Ceperly Adler Perdew and Zunger (LDA-CAPZ). One of the purposes of selecting cobalt as a doping atom is its highly effective charge on the Co atom, which can boost the electrical conductivity and enhance the performance of energy storage devices. This work required the convergence test, and *k*-point values were conducted to ensure the accuracy of the calculations. The lattice parameters of pure α-NiS crystal structure are in the hexagonal space group (*P63/mmc*), which displays a good agreement compared with the previous experimental work. The average bond length for pure NiS increases with the supercell Co-doped α-NiS crystal structure. For electronic properties, the energy band gap of pure and Co-doped α-NiS shows a good result which contributes higher than the experimental band gap. These results have been done with the recognition of Hubbard *U* value after the supercell crystal structure displays a lower energy band gap. The electronic charge distribution of pure and Co-doped α-NiS are also illustrated to identify whether the bonding characteristics are ionic or covalent bonds. The density of states represents the hybridization state of Co 3*d*, Ni 3*d,* and S 3*p* orbitals at the conduction band (CB) and valence band (VB). The bonding populations refer to the bonding characteristics of pure and Co-doped α-NiS.

Keywords: First principles; density functional theory; Co-doped α-NiS; structural properties; electronic properties

INTRODUCTION

Nickel sulfides (NiS), one of the transition metal sulfides family, encapsulates two different types of polymorphs, which is nickeline (α-NiS) and millerite (ß-NiS) [1,2]. Some metal sulfides have a variety of polymorphs phase which is similar to NiS, such as copper sulfide (CuS) [3], cadmium sulfide (CdS) [4], and cobalt sulfide (CoS) [5]. Based on both phases, the pure nickeline NiS contributes an important role, especially in energy storage applications, due to its p-type character behaviour and enhances the energy band gap of ~0.5 eV compared to millerite NiS [6]. In addition, many researchers are interest in both phases of NiS, especially in structural and electronic properties [7-9]. Sparks and Komoto reported that NiS forms with a hexagonal structure and can be maintained by quenching it to room temperature. When the temperature is further cooled, the hexagonal NiS undergoes a first-order metal-nonmetal transition at the transition temperature of about 260 K [10]. The high-temperature (HT) phase reacts as a paramagnetic metal, whereas the low-temperature (LT) phase is an antiferromagnetic semiconductor [11,12]. The magnetic structure of α-NiS is illustrated as in Figure 1 below where they found that the magnetic moments of Ni atoms are coupled ferromagnetically (FM) within (001) layers whereas the moments on adjacent layers are coupled antiferromagnetically (AFM).

Recently, nickeline is still one of the significant applications due to its structural stability and promising a lower energy band gap compared to millerite. In addition, the optical reflectivity spectra nickeline has been measured and it was found that the non-metallic phase is a carrier-doped semiconductor with an energy gap of 0.2 ~ 0.3 eV [13]. Furthermore, Wu et al. reported the phase engineering of NiS via a theoretical and experimental method where it can be clarified that hexagonal nickeline NiS has a better mechanical capability, is more conducive to ion absorption and conduction and generates a high pseudocapacitive contribution [14]. These features contributed a lot of potential and more interest towards exploring this material in storage devices. Some of the storage applications implement hexagonal nickeline phases, such as solar energy systems [15], photocatalytic hydrogen evolution [16], supercapacitors energy storage [17], and photodetector [18].

NiS is highly attractive due to the high theoretical capacitance, rich redox activity, and rich electroactive sites [19-21]. However, it is known that single nickeline NiS suffers from two drawbacks which are poor high-rate performance and short cycling stability. These drawbacks may be affected by the low electrical conductivity where this microstructure was applied to lubricate the electron charge transfer process [22, 23]. Therefore, developing Co-doped NiS is the foremost strategy to overcome the limitations. Introducing the Co doping atom may influence the electronic properties of the nickeline NiS phase, hence promising higher conductivity and reducing the electrochemical polarization at higher current and power density [24,25]. Most researchers were captivated after observing the effect of Co doping atoms toward nickeline NiS.

The fundamental understanding of doping Co atom towards nickeline NiS is still lacking. The density functional theory (DFT) in the present first-principles study is applied to obtain the original objectives. This paper aims to study the effect of Co dopedNiS as a semiconductor material. This paper will highlight the theoretical calculations related to electronic band structure, electron charge distribution, and total and partial density of states. This paper also permits the other researchers to explore the material's theoretical part in detail.

MATERIALS AND METHODS

In this study, all computations were performed in Materials Studio (MS) 8.0 software using the Cambridge Serial Total Energy Package (CASTEP) computer code based on DFT. For general energy, the ultra-soft pseudopotential technique has been utilized. The electronic wave function is unraveled using plane wave base groups, and the ion potential is supplanted with ultra-soft pseudopotential. Some common exchange-correlation was functional such as local density approximation by Ceperly Adler Perdew and Zunger (LDA-CAPZ), generalized gradient approximation of Perdew-Burke-Ernzenhof (GGA-PBE), and Perdew-Burke-Ernzerhof for solids (GGA-PBEsol) were used. The practical *U* values for nickeline (α-NiS) from LDA+U are 8 eV, which can be described as the optimal outcome of *U* values compared to the other studies with different approach calculations from various kinds of computer code. The attributes of *U* have been estimated from the electronic properties calculations [26,27,28]. The following formalism was used to characterize the calculated structural and electronic properties of the NiS polymorph using LDA+U with the firm, effective on-site Coulomb repulsion among the localized Ni 3d electrons:

$$E_{DFT+U} = E_{DFT} \frac{(U-J)}{2} \sum_{\sigma} Tr(\rho^{\sigma} - \rho^{\sigma}\rho^{\sigma}) \quad (1)$$

where *U* and *J* are the Coulomb and exchange energy, respectively and ρ^{σ} refers to the spin (σ) polarized-on-site density matrix. The convergence test of cut-off and k-points for the pure and doping structure was carried out and set up with 330 eV and 4×4×2. The convergence threshold is one the most important in conducting the calculation with the setup for the pure structure of 5.0×10^{-6} eV/atom for energy change, the maximum force of 0.01 eV/Å, the maximum stress of 0.02 GPa and maximum displacement of 5.0×10^{-4} Å. The Co, Ni, and S valence electronic configurations were [Ar] $3d^7$, [Ar] $3d^{8,}$ and [Ne] $3s^2$ $3p^6$, respectively.

RESULTS AND DISCUSSION

Structural Properties

The pure α-NiS 1×1×1 unit cell structure was studied, and the geometry-optimized crystal structure is illustrated in Figure1. In contrast, Table 1 shows the optimized lattice parameters, cell volume, and cell angle of both pure α-NiS and Co-doped α-NiS. The lattice parameters for pure α-NiS were compared with the experimental results, whereas the lattice parameters of Co-doped α-NiS were compared with the theoretical results. Generally, the lattice parameters, cell volume, and cell angles of pure α-NiS unit cell crystal structure indicate a slight difference after comparing with the experimental data. In addition, the lattice constants *a*=*b* exceeded about 0.58%, while the lattice constant *c* gained an underestimated percentage error of 2.85%. The pure α-NiS crystal structure volume recorded a minimized percentage error of 1.52% compared to the experimental results by summing up the percentage error of lattice constants *a*, *b* and *c*. This unit cell crystal structure results significantly show the changes of lattice parameters after doping with the Co atom due to the different number of ionic radii where Co^{2+} (0.72 Å) is shorter than Ni^{2+} (0.78 Å) [29]. Hence, it also enlarges the crystal structure's size and may affect the magnetic parameters of NiS material [30, 31].

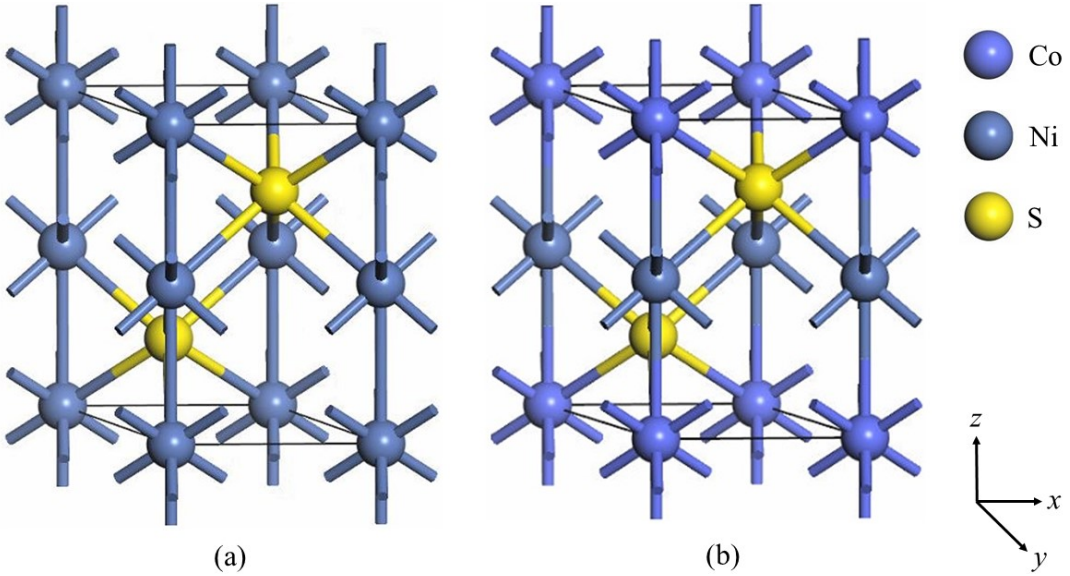

Figure 1. Crystal structure of (a) pure α-NiS and (b) Co-doped α-NiS in 1×1×1 unit cell

Table. 1. Calculated lattice parameters (*a*, *b* and *c*), cell volume, and cell angle for pure NiS and Co-doped NiS in 1×1×1 unit cell

Structures	Parameters (Å)	LDA-CAPZ	Experiment
NiS	*a*	3.459 (+0.58%)	3.439
	b	3.459 (+0.58%)	3.439
	c	5.198 (-2.85%)	5.351
	Cell Volume ($Å^3$)	53.860 (-1.52%)	54.692
	Cell Angle (°)	α = 90	α = 90
		ß = 90	ß = 90
		γ= 120	γ= 120
Co-doped NiS	*a*	3.428 (-0.90%)	-
	b	3.428 (-0.90%)	-
	c	5.336 (+2.65%)	-
	Cell Volume ($Å^3$)	54.233 (+0.69%)	-
	Cell Angle (°)	α = 90.04	-
		ß = 89.96	-
		γ= 120.11	-

The magnetic structures of α-NiS are illustrated in Table 2. As a result, it indicates that the energy of AFM order of α-NiS obtained is lower than that of the FM order due to the cancellation of spin direction between 2 layers. This result is in agreement with the findings from Barthelemy et al., where they concluded that α-NiS behaves as an AFM order with ferromagnetically coupled between the layers and antiferromagnetically coupled at the adjacent layer [32].

Table 2. Magnetic structure of α-NiS with its order and energy obtained from the calculations

Magnetic Structure	Order	Energy (eV)	Magnetic Moment (μ_B)
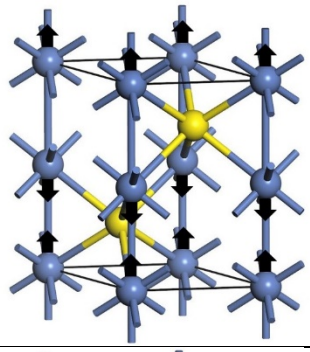	Antiferromagnetic	-3256.3287	$\mu_{B,\ Ni} = \mu_{B,\ S} = 0$
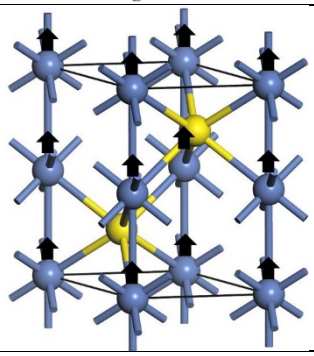	Ferromagnetic	-3255.1191	$\mu_{B,\ Ni} = 0.74$ $\mu_{B,\ S} = 1.26$

Average Bond Length

The calculated average bond length for pure α-NiS and Co-doped NiS of 1×1×1 unit cell was tabulated as in Table 3. In this calculation, we are focusing on the Ni – S bond for the unit cell and the Co – S bond for the supercell to determine the bonding behaviour of α-NiS materials. According to the periodic table of elements, Co is located beside Ni in the transition metal elements group because Co atom is larger than the Ni atom. Therefore, the 1×1×1 unit cell results show that the Ni – S bond is longer than the doping crystal structure. In addition, the Co – S bond in the doping crystal structure was recorded longer than the Ni – S bond. These results indicate that doping the Co atom increases the lattice parameters and extends the bond length of NiS material in a 1×1×1 unit cell crystal structure. Hence, the Co – S behaves weaker than the Ni – S bond.

Table 3. Average bond length for pure α-NiS and Co-doped α-NiS in 1×1×1 unit cell

Parameters	1×1×1 Unit Cell	
	Pure α-NiS	Co-doped α-NiS
Ni – S (Å)	2.383	2.368
Ni – Ni (Å)	2.599	3.427
Co – S (Å)	-	2.402

Band Structures

This section will explore the electronic structure properties used to identify the band structure and total and partial density of states (DOS) of α-NiS. Nickel sulfide obtains an indirect band gap of 0.2-1.2 eV for experimental and theoretical findings [33-35]. This transition metal sulfide (TMS) group has drawn much attention because of its

fundamental characteristics, practical uses, and contribution to deep material circulation [36].

The energy band gap is usually calculated between the conduction band minimum (CBM) and valence band maximum (VBM), located at the Fermi level. The high-symmetry Brillouin Zone electronic structure of pure α-NiS in 1×1×1 unit cell is illustrated in Figure 2. By considering the effect of U parameters towards the NiS structure, the selected U values towards pure and doping crystal structure were conducted and clarified from the variations of U_d and U_p values as illustrated in Figure 3 with the range of U values taken from 8 eV to 11 eV for both U_d and U_p. As a result, we can see that the $U_{d, Ni}$ = 8 eV, and $U_{p, S}$ = 8 eV, are selected as the best value where the energy band gap at this point is closer to the experimental band gap. The pure and doping electronic structures were already inserted with Hubbard U value which is $U_{d, Ni} = U_{p, S}$ = 8 eV and $U_{d, Co}$ = 12 eV, $U_{d, Ni} = U_{p, S}$ = 8 eV, respectively. The band structure of the pure and doping form is displayed in Figure 4. The reason for applying Hubbard U to the Co, Ni, and S atoms is to make some corrections at or near the Fermi level. Based on the results, pure α-NiS display an indirect band gap at the Fermi level, which is 0.523 eV. This result is in agreement with the experimental band gap, which is 0.5 eV. After doping the Co atom at the lowest energy position, the indirect energy band gap increased to 1.4 eV. It indicates that the doping Co atom, which replaces the Ni sites, influences the energy band gap and may produce almost two times the pure energy band gap.

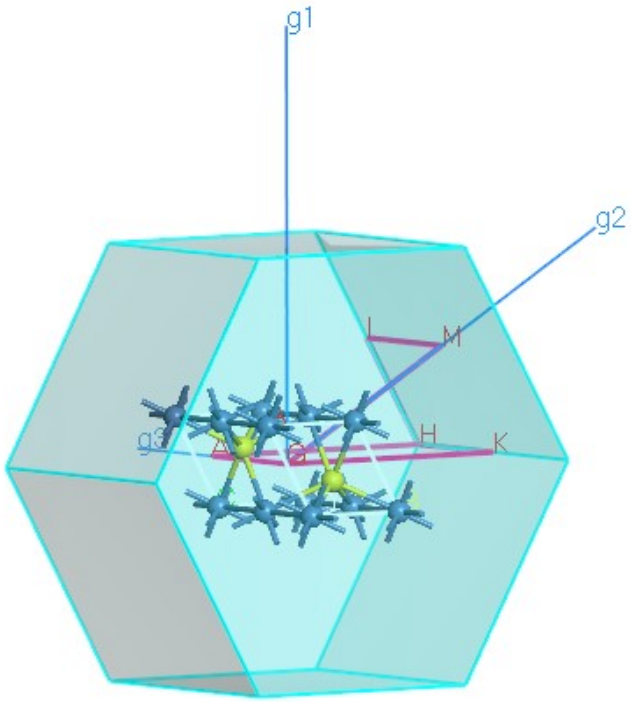

Figure 2. High-symmetry Brillouin Zone electronic structure of pure α-NiS in 1×1×1 unit cell

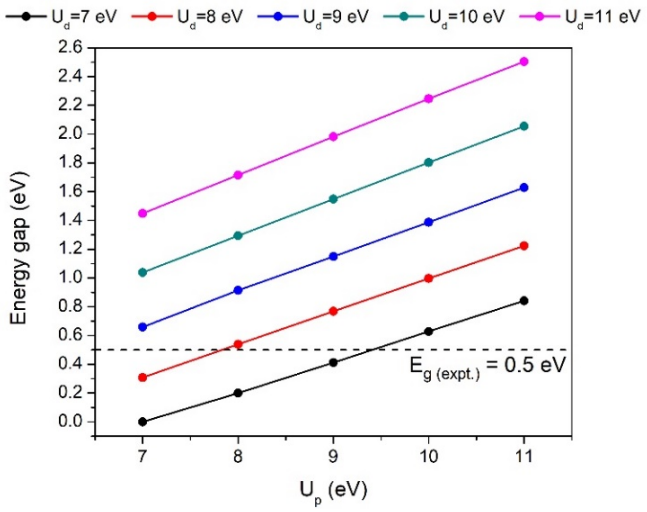

Figure 3. Variations of the energy band gap of NiS with different Hubbard U_p value

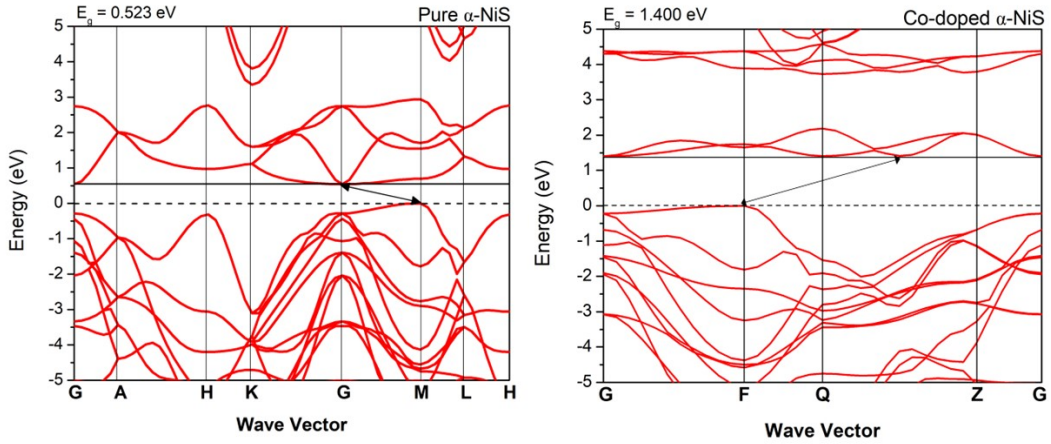

(a) (b)

Figure 4. Band structure of (a) pure α-NiS and (b) Co-doped α-NiS in 1×1×1 unit cell

Density of States (DOS)

Density of states (DOS) calculation was computed to determine the contributions of orbitals in each atom of the crystal structure. The DOS for the pure and doping forms are displayed in Figure 5. Based on the figure, we can see that the Ni-3*d* orbital started to be fulfilled at the valence band region, which is between -10 eV and -5 eV, whereas the S-3*p* orbital was dominant also at the valence band region. The highest peak recorded in the pure calculation is Ni-3*d* orbital, with 7.6 electrons per eV. This result also can indicate the energy band gap of the refined structure, which is 0.523 eV, with the correction of Hubbard *U* that applies to Ni-3*d* and S-3*p* orbitals.

For Co-doped α-NiS, the Co-3*d* orbital was dominant far from the Fermi energy level. Furthermore, the highest peak recorded is 4.5 electrons per eV, located at the conduction band region in the range of energy between 0 eV and 5 eV. The Ni-3*d* and S-3*p* orbitals contribute similar results as in the pure structure, which is dominant at the valence band region. In addition, the S-3*p* in the both sophisticated and doping system can be classified as the determinant orbitals where it hybridizes near the Fermi energy level and hence determine the value of the energy band gap. Overall, the DOS

of pure and doping have different contributions in orbitals. Moreover, the Co doping atom can change the delocalization of *pd* orbitals in NiS material.

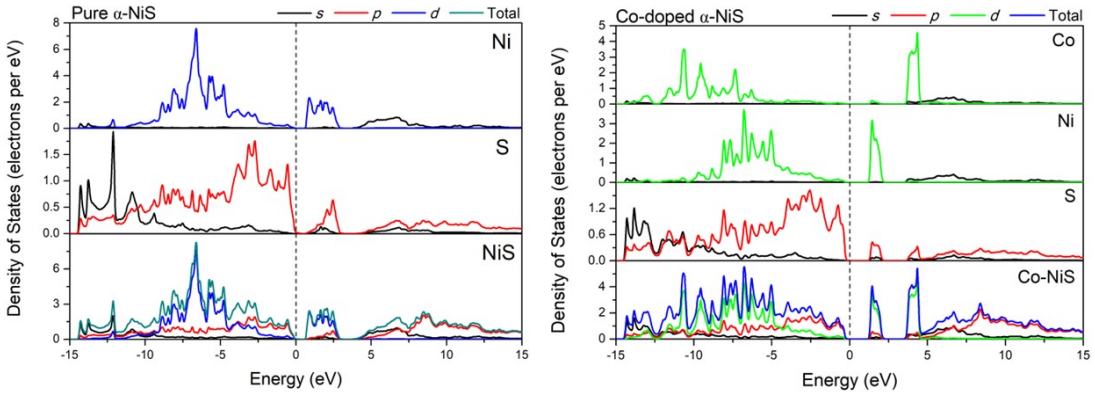

(a) (b)

Figure 5. DOS of (a) pure α-NiS and (b) Co-doped α-NiS in 1×1×1 unit cell

Electron Charge Density

The electronic charge distribution indicates the contribution of electrons around the specific atoms and determines whether the crystal structure model behaves as ionic or covalent bonds. Figure 6 illustrates the distribution of different structures' electron density in pure and Co-doped α-NiS. To describe the bonding characteristic of both forms, Table 4 shows the range of specific values representing certain bonding characteristics. The results indicate that pure α-NiS contributes a robust covalent bond before doping into the Ni site. This is because the Ni and S atoms were located at the solid covalent region near the green color.

On the other hand, the bond population analysis for pure α-NiS is 0.80, located in the range of 0.75 to 1 based on the indicator table below. However, for doping structure, it behaves as a "close to covalent" bonding characteristic due to the value of bond population, which is 0.72. From the mapping color, the Co and S atoms were situated in the yellow region, which agreed with the results obtained from the calculation. This value is located in the range between 0.5 and 0.7. The justification for these results is the Co^{2+} dopant may influence the bonding characteristics of α-NiS before and after doping. In addition, it also may differ the value of bond population at Ni – S and Co – S bonds.

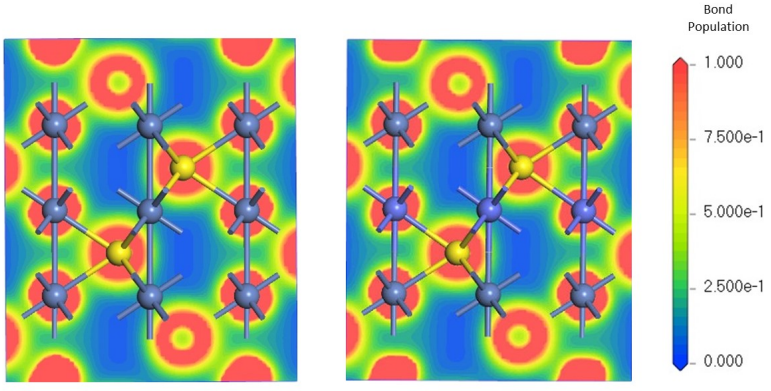

(a) (b)

Figure 6. Electron charge distribution for (a) pure α-NiS and (b) Co-doped α-NiS in 1×1×1 unit cell

CONCLUSIONS

In summary, the structural and electronic properties of pure and Co-doped α-NiS in unit cell crystal structure determined using the DFT and DFT+U method provide a good agreement compared to the experimental data. The standard DFT calculation is unreliable because it cannot fix the delocalization of orbitals in α-NiS semiconductor material. Therefore, the Hubbard *U* correction has occurred by setting the *pd* orbitals for Co, Ni, and S atoms. The lattice constants *a*, *b,* and *c* of pure α-NiS are longer than Co-doped α-NiS with less percentage error. The Hubbard *U* correction method does not affect the structural properties of pure and Co-doped α-NiS as it is more focused on the electronic part, which is the energy band gap and density of states. Therefore, the energy band gap for pure and Co-doped α-NiS, including the Hubbard *U* value, gained an energy gap of 0.523 eV and 1.400 eV, respectively. This shows that doping of Co in α-NiS crystal structure increases the energy band gap. The DOS calculation shows strong hybridization of the Co-3d, Ni-3d, and S-3p orbitals, especially at the valence band region. The study of pure α-NiS and Co-doped α-NiS can be enhanced with supercell crystal structure and different doping concentration values where the results can be precise. Also, it may justify the effect of doping Co towards α-NiS crystal structure.

ACKNOWLEDGMENTS

This work was supported by the Universiti Teknologi MARA under UiTM Excellent Fund (600-RMC/KEPU 5/3 (008/2021)). Most Ionics, Materials, and Devices (iMADE) Research Laboratory, Institute of Science (IOS), UiTM for the facilities provided.

REFERENCES

[1] Y. Ouyang, Y. Chen, J. Peng, J. Yang, C. Wu, B. Chang, X. Guo, G. Chen, Z. Luo, X. Wang (2021). Nickel sulfide/activated carbon nanotubes nanocomposites as advanced electrode of high-performance aqueous asymmetric supercapacitors, *Journal of Alloys and Compounds* **885**, 160979.

[2] S.R. Krishnakumar, N. Shanthi, D.D. Sarma (2002). Electronic structure of millerite NiS, *Physical Review B* **66**, 115105.

[3] C. An, S. Wang, J. He, Z. Wang (2008). A composite-surfactants-assisted-solvothermal process to copper sulfide nanocrystals, *Journal of Crystal Growth* **310**, 266.

[4] L. Dhatchinamurthy, P. Thirumoorthy, L. Arunraja, S. Karthikeyan (2020). Synthesis and characterization of cadmium sulfide (CdS) thin film for solar cell applications grown by dip coating method, *Materials Today: Proceedings* **26**, 3595.

[5] B. Li, L.Y. Cao, J.F. Huang, J.P. Wu (2012). Synthesis of Cobalt Sulfide Nanocrystallites via an Efficient Microwave Hydrothermal Process, *Key Engineering Materials* **512-515**, 162.

[6] R. Boughalmi, R. Rahmani, A. Boukhachem, B. Amrani, K. Driss-Khodja, M. Amlouk (2015). Metallic behavior of NiS thin film under the structural, optical, electrical and ab initio investigation frameworks, *Materials Chemistry and Physics* **163**, 99.

[7] S. Iram, A. Mahmood, M.F. Ehsan, A. Mumtaz, M. Sohail, E. Sitara, S.A.B. Bukhari, S. Gul, S.A. Fatima, M.Z. Khan, R. Shaheen, S.N. Malik, M.A. Malik (2021). Impedance spectroscopic study of nickel sulfide nanostructures deposited by aerosol assisted chemical vapor deposition technique, *Nanomaterials* **11**, 1105.

[8] J. Yoo, I.H. Kwak, I.S. Kwon, K. Park, D. Kim, J.H. Lee, S.A. Lim, E.H. Cha, J. Park (2020). Nickel sulfide nanocrystals for electrochemical and photoelectrochemical hydrogen generation, *Journal of Materials Chemistry C* **8**, 3240.

[9] X.K. Zhang, J.Y. Li, J.C. Lin, P. Tong, M. Wang, X.L. Wang, H.Y. Tong, Y.S. Zhang, W.H. Song, Y.P. Sun (2021). High-contrast, reversible change of thermal conductivity in hexagonal nickel-iron sulfides, *Acta Materialia* **208**, 116709.

[10] J.T. Sparks, T. Komoto (1963). Neutron diffraction study of NiS, *Journal of Applied Physics* **34**, 1191-1192.

[11] S. Anzai, J. Ozawa (1968). Effect of pressure on the magnetic and electrical transition point of the NiAs-type NiS, *Journal of the Physical Society of Japan* **24**, 271-274.

[12] J.T. Sparks, T. Komoto (1967). Metal-to-semiconductor transition at the magnetic ordering temperature of NiS, *Physics Letters* **25**, 398-399.

[13] H. Okamura, J. Naitoh, T. Nanba, M. Matoba, M. Nishioka, S. Anzai, I. Shimoyama, K. Fukui, H. Miura, H. Nakagawa, K. Nakagawa, T. Kinoshita (1999). Optical study of the metal–nonmetal transition in Ni1⩾dS, *Solid State Communications* **112**, 91-95.

[14] J. Wu, S. Liu, Y. Rehman, T. Huang, J. Zhao, Q. Gu, J. Mao, Z. Guo (2021). Phase engineering of nickel sulfides to boost sodium- and potassium-ion storage performance, *Advanced Functional Materials* **31**, 2010832.

[15] D. Sathya (2022). NiS thin films for solar cell applications by successive ionic layer adsorption and reaction (silar) method, *GIS Science Journal* **9**, 89.

[16] M. Muniyappa, S. N. Kalegowda, M. Shetty, J.B. Sriramoju, M. Shastri, S.V. Navakoteswara Rao, D. De, M.V. Shankar, D. Rangappa (2022). Cocatalyst free nickel sulphide nanostructure for enhanced photocatalytic hydrogen evolution, *International Journal of Hydrogen Energy* **47**, 5307.

[17] A. Gahtar, S. Benramache, A. Ammari, A. Boukhachem, A. Ziouche (2021). Effect of molar concentration on the physical properties of NiS thin film prepared by spray pyrolysis method for supercapacitors, *Inorganic and Nano-Metal Chemistry* **52**, 1-10.

[18] N. Abhiram, D. Thangaraju, R. Marnadu, G. Johnsy Arputhavalli, S. Gunasekaran, P. Vetrivelan, N.S.M.P. Latha Devi, M. Shkir, H. Algarni (2021). Structural, vibrational, morphological, optical and electrical properties of NiS and fabrication of SnS/NiS nanocomposite for photodetector applications, *Inorganic Chemistry Communications* **133**, 108882.

[19] T.V. Nguyen, L.T. Son, P.M. Thao, L.T. Son, D.T. Phat, N.T. Lan, N.V. Nghia, T.V. Thu (2020). One-step solvothermal synthesis of mixed nickel–cobalt sulfides as high-performance supercapacitor electrode materials, *Journal of Alloys and Compounds* **831**, 154921.

[20] Z. Ma, Z. Sun, H. Jiang, F. Li, Q. Wang, F. Qu (2020). Nanoporous electrospun $NiCo_2S_4$ embedded in carbon fiber as an excellent electrode for high-rate supercapacitors, *Applied Surface Science* **533**, 147521.

[21] N. Poompiew, P. Pattananuwat, P. Potiyaraj (2021). In situ hydrothermal synthesis of nickel cobalt sulfide nanoparticles embedded on nitrogen and sulfur dual

doped graphene for a high performance supercapacitor electrode, *RSC Advances* **11**, 25057.

[22] Y. Li, J. Li, M. Wang, Y. Liu, H. Cui (2019). High rate performance and stabilized cycle life of Co^{2+}-doped nickel sulfide nanosheets synthesized by a scalable method of solid-state reaction, *Chemical Engineering Journal* **366**, 33.

[23] B. Pant, G.P. Ojha, M. Park (2020). One-pot synthesis, characterization, and electrochemical studies of tin-nickel sulfide hybrid structures on nickel foam for supercapacitor applications, *Journal of Energy Storage* **32**, 101954.

[24] J. Hu, L. Zhao, Y. Chu, Q. Tian, J. Wang, Y. Li, Q. Wu, Y. Zhu (2018). Preparation and electrochemical properties of a new $Fe_{0.5}Co_{0.5}S_2$ cathode material for thermal batteries, *Journal of Alloys and Compounds* **762**, 109.

[25] H. Guo, L. Tang, Q. Tian, Y. Chu, B. Shi, X. Yin, H. Huo, X. Han, C. Yang, C. Wang, K. Tang, C. Wang, X. Zhang, J. Wang, L. Kong, Z. Lu (2020). Cobalt-Doped NiS_2 Micro/Nanostructures with Complete Solid Solubility as High-Performance Cathode Materials for Actual High-Specific-Energy Thermal Batteries, *ACS Appl Mater Interfaces* **12**, 50377.

[26] M. Usuda, N. Hamada (1999). Empirical LSDA+U Study for Electronic Structure of Hexagonal NiS, *Journal of the Physical Society of Japan* **69,** 744-748.

[27] N. Jiang, Q. Tang, M. Sheng, B. You, D.-e. Jiang, Y. Sun (2016). Nickel sulfides for electrocatalytic hydrogen evolution under alkaline conditions: a case study of crystalline NiS, NiS_2, and Ni_3S_2 nanoparticles, *Catalysis Science & Technology* **6**, 1077.

[28] S.K. Panda, P. Thunström, I.D. Marco, J. Schött, A. Delin, I. Dasgupta, O. Eriksson, D.D. Sarma (2014). A charge self-consistent LDA+DMFT study of the spectral properties of hexagonal NiS, *New Journal of Physics* **16**, 093049.

[29] S.M. Kabbur, S.D. Waghmare, U.R. Ghodake, S.S. Suryavanshi. (2018) Synthesis, morphology and electrical properties of Co^{2+} substituted NiCuZn ferrites for MLCI applications, *AIP Conference Proceedings* **1942,** 130002.

[30] M.M. Obeid, S.J. Edrees, M.M. Shukur (2018). Synthesis and characterization of pure and cobalt doped magnesium oxide nanoparticles: Insight from experimental and theoretical investigation, *Superlattices and Microstructures* **122**, 124.

[31] S. Debnath, A. Das, R. Das (2021). Effect of cobalt doping on structural parameters, cation distribution and magnetic properties of nickel ferrite nanocrystals, *Ceramics International* **47**, 16467.

[32] E. Barthelemy, O. Gorochov, H. McKinzie (1973). The electrical and magnetic properties of the transition in nickel sulfide, *Materials Research Bulletin* **8**, 1401.

[33] S.D. Sartale, C.D. Lokhande (2001). Preparation and characterization of nickel sulphide, *Materials Chemistry and Physics* **72**, 101.

[34] S.K. Panda, I. Dasgupta, E. Sasioglu, S. Blugel, D.D. Sarma (2013). NiS - an unusual self-doped, nearly compensated antiferromagnetic metal, *Sci. Rep.* **3**, 2995.

[35] W.B. Zhang, J. Li, B.Y. Tang (2013). Role of electronic correlation in high-low temperature phase transition of hexagonal nickel sulfide: a comparative density functional theory study with and without correction for on-site Coulomb interaction, *J Chem Phys* **138**, 244703.

[36] Q. Zhang, Y. Tian, S. Liu, P. Yang, Y. Li (2020). First-Principles Study of the Elastic Properties of Nickel Sulfide Minerals under High Pressure, *Minerals* **10**, 737.